Subwavelength optical lithography via classical light: A possible implementation

Jieyu You,[1] Zeyang Liao,[1] P. R. Hemmer,[2] and M. Suhail Zubairy[1]
[1]*Institute for Quantum Science and Engineering (IQSE) and Department of Physics and Astronomy, Texas A&M University, College Station, Texas 77843-4242, USA*
[2]*Department of Electrical Engineering, Texas A&M University, College Station, Texas 77843, USA*

(Received 19 January 2018; published 6 April 2018)

The resolution of an interferometric optical lithography system is about the half wavelength of the illumination light. We proposed a method based on Doppleron resonance to achieve a resolution beyond half wavelength [Phys. Rev. Lett. **96**, 163603 (2006)]. Here, we analyze a possible experimental demonstration of this method in the negatively charged silicon-vacancy (SiV^-) system by considering realistic experimental parameters. Our results show that quarter wavelength resolution and beyond can be achieved in this system even in room temperature without using perturbation theory.

DOI: 10.1103/PhysRevA.97.043807

I. INTRODUCTION

Optical lithography is widely used to print a circuit image onto a substrate [1]. When a portion of the photoresist is exposed to the light, it becomes soluble (or insoluble) to the photoresisit developer so that a desired pattern can be formed [2]. However, for noncontact optical lithography diffraction limits the minimum feature size to about half the optical wavelength [3]. To print smaller features, the illumination source should be reduced from visible light to extreme ultraviolet (EUV) or even x ray. However, the air can absorb the EUV and x ray significantly and therefore it requires operation in a vacuum system. In addition, the traditional lense used for visible light does not work for short wavelength. Moreover, the photon energies of the EUV and x ray are so high that they may damage the silicon substrate [4]. Thus it is desirable to invent a method to overcome the diffraction limit in the optical lithography [5,6].

In the past two decades, a number of methods have been proposed to achieve superresolution in optical lithography, including the methods based on quantum entanglement [7–9], quantum dark state [10–12], Rabi oscillations [13–15], coherent atom lithography [16–18], and magnetic resonance [19]. Although quantum entanglement can successfully suppress the diffraction-limited resolution term and achieve a $\lambda/2N$ resolution, it is hard to experimentally generate sufficiently bright and pure NOON states [20]. In 2006, we proposed a method based on Doppleron resonance which can mimic the effect of quantum entanglement and achieve superresolution but using only classical light [21]. Compared to the usual multiphoton absorption process [22], our method based on Doppleron resonance can have a higher efficiency and visibility. In addition, our method is in principle able to print an arbitrary super-resolved pattern, but a suitable material for demonstrating the method is still unknown [23,24]. Here, we study a possible experimental realization of this method using silicon vacancy (SiV) in diamond. One big advantage of SiV is that it has 70% of its fluorescence in 738 nm zero-phonon line (ZPL) [25,26]. By numerically solving the dynamics of these systems using realistic material parameters, we show that a factor of 2 and beyond resolution enhancement can be achieved. While this may not seem impressive by itself, it will demonstrate the feasibility of the technique and new color centers are continually being discovered that may outperform the SiV, for example, the germanium-vacancy (GeV) center in diamond.

This paper is organized as follows: In Sec. II, we briefly introduce the scheme for subwavelength optical lithography via the Doppleron effect. In Sec. III we briefly introduce the SiV^-'s electronic structure and then show how to use it to write a subwavelength pattern. In Sec. IV, we make a realistic calculation based on the existing experimental data. We include decay in our calculations and show that a $\lambda/4$ resolution can be generated. Finally, we summarize the results.

II. SUBAWAVELENGTH OPTICAL LITHOGRAPHY WITH CLASSICAL LIGHT

In this section, we first briefly show how to achieve subwavelength optical lithography via the Dopperlon effect. The schematic setup is shown in Fig. 1 where four-level atoms interact with two classical light beams. Two signal laser beams with slightly different frequencies ($\nu_\pm$) are incident from opposite directions in plane and two drive beams with frequency $\omega_\pm$ are incident from the normal direction. The resonant excitation from ground state $|g\rangle$ to excited state $|e\rangle$ can be reached by either absorbing two photons from the left with frequency ν_+ and one photon from the drive field with frequency ω_+ or absorbing two photons from the right with frequency ν_- and one photon from the drive field with frequency ω_-, i.e., $\omega_{ab} = 2\nu_\pm - \omega_\pm$. Other combinations of absorption are negligible due to the lack of resonance. By satisfying these conditions, the four-level atoms are either absorbing two photons from the left or two photons from the right but never one photon from the left and one photon from the right [21]. Such resonances were observed in atoms moving in an intense standing-wave field where multiphoton resonances were observed at certain velocities or Doppler shifts, hence the name. By selective absorption of specific

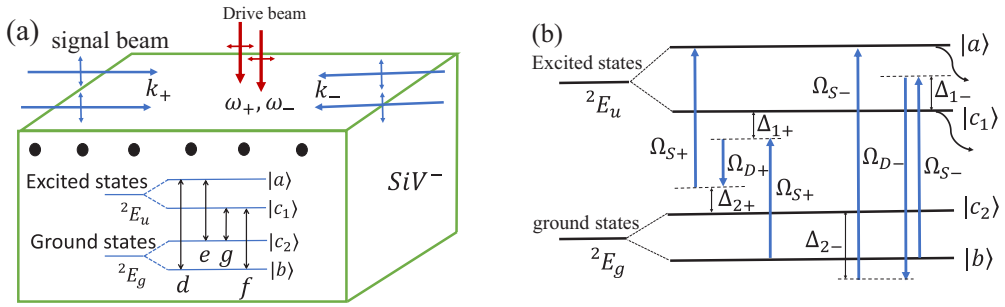

FIG. 1. (a) The schematic setup of subwavelength optical lithography via classical light. Two signal beams are incident at a very small angle to ensure that the polarization is perpendicular to the {111} surface, so the signal frequencies can only excite e and f transitions. The drive beams are normally incident to the surface. Two drive fields mainly excite transition g rather than d due to the big detuning between the drive frequency and transition frequency of d. (b) Electronic pumping from the ground state to the excited state, where $\Omega_{D\pm}$ is $k_\pm$'s contribution to transition f and e. Here we only show the resonant pumping (zero multiphoton detuning).

Fock states from intense classical light, this effect can mimic quantum entanglement. The absorption rate is proportional to

$$|e^{2ikx} + e^{-2ikx}| \sim \cos(4kx). \tag{1}$$

The period of the pattern is $\lambda/4$ and therefore the resolution is enhanced by a factor of two. By generalizing this system to more energy levels and more drive beams, we can in principle improve the resolution beyond a factor of two. Therefore, we can achieve the same resolution as the quantum NOON state by just using classical light.

Despite the simplicity of this scheme, no experiment has been done yet. One main reason is the lack of a suitable material for demonstrating this method. In the following, we propose and numerically show that SiV may be a good candidate material for subwavelength optical lithography based on Doppleron resonance. Due to their similarities in symmetries and electronic structure, our arguments can also be applied to other color centers like NV and GeV [27,28].

III. PROPOSED EXPERIMENTAL SETUP

The proposed experimental setup is shown in Fig. 1(a) where a shallow layer of SiV^- centers is oriented in the (111) direction (i.e., perpendicular to the diamond surface). Although such an oriented layer of SiV has not yet been observed, a microwave plasma-assisted chemical vapor deposition diamond growth technique on (111)-oriented substrates in NV is reported [29]. Due to the similarities in symmetries and electronic structure, it is therefore possible to fabricate such a layer for SiV. The electronic structure of the SiV^- center is also shown in Fig. 1(a) with ground doublet levels ^2E_g and excited doublet levels ^2E_u [30]. For simplicity, we relabel the four doublet states as $|a\rangle, |c_1\rangle, |c_2\rangle, |b\rangle$. The dipole directions of the transitions f and e are along the [111] crystal vector, and the dipoles of transitions d and g are perpendicular to the [111] crystal vector. Due to the symmetry, d's and g's dipoles have the same magnitude in every direction perpendicular to [111] [31]. The relative magnitude of four dipole moments can also be inferred from the photoluminescence intensity in Ref. [31], where the photoluminescence intensity is proportional to the modulus square of the transition dipole after correcting for Boltzmann population differences. Therefore, all the four transition dipoles have similar strengths. As in Ref. [21], we need pairs of drive beams and signal beams to complete three-photon resonance in each of the two opposite directions. As shown in Fig. 1(a), signal beams are incident at a small angle with polarizations almost perpendicular to the surface and wave vectors k identical along the surface. Therefore, those signal beams only excite the transitions f and e and produce a diffraction-limited periodic pattern. The drive beams are normally incident with their polarizations perpendicular to the [111] direction so that they are coupled to transitions g and d. The level structure and beam coupling are shown in Fig. 1(b) where multiphoton resonance is achieved by absorbing two photons from signal beams of the same incident direction and one from the drive beam.

In the rotating wave approximation (RWA) and the interaction picture, the interaction Hamiltonian including four signal beams is given by

$$\begin{aligned} H_I = &-\frac{\hbar}{2}\sum_{\alpha=\pm}(\Omega_{S\alpha}|c_1\rangle\langle b|e^{i(-\nu_\alpha t+\omega_{bc_1}t+\alpha kx)} \\ &+\Omega_{S\alpha}|a\rangle\langle c_2|e^{i(-\nu_\alpha t+\omega_{ac_2}t+\alpha kx)} \\ &-\frac{\hbar}{2}\sum_{\alpha=\pm}(\Omega_{D\alpha}|c_1\rangle\langle c_2|e^{i(-\nu_{D\alpha}t+\omega_{c_1c_2}t)} \\ &+\Omega_{D\alpha}|a\rangle\langle b|e^{i(-\nu_{D\alpha}t+\omega_{ab}t)}) + \text{H.c.}, \end{aligned} \tag{2}$$

where the Rabi frequencies are set to be $\Omega_{S\pm} = |\mu|E_S/\hbar$ and $\Omega_{D\pm} = |\mu|E_D/\hbar$ (we have the relationship $\mu_{ac_2} \approx \mu_{bc_1} \approx \mu_{ab} \approx \mu_{c_1c_2} \approx \mu$), and the index $S(D)$ is short for "signal"("drive"). For simplicity, we have set the transition dipole moment to be real, while it is not necessary to do so because the phase of the dipole moment will not yield any differences in observation. We define the detunings as follows: $\Delta_{1\pm} = \omega_{c_1b} - \nu_\pm$, $\Delta_{2\pm} = \omega_{ac_2} - \nu_\pm$, $\omega_{ij} = |E_i - E_j|/\hbar$.

IV. NUMERICAL CALCULATION

The master equation of the system is given by

$$\dot{\rho} = -\frac{i}{\hbar}[H_I, \rho] + \mathscr{L}[\rho], \tag{3}$$

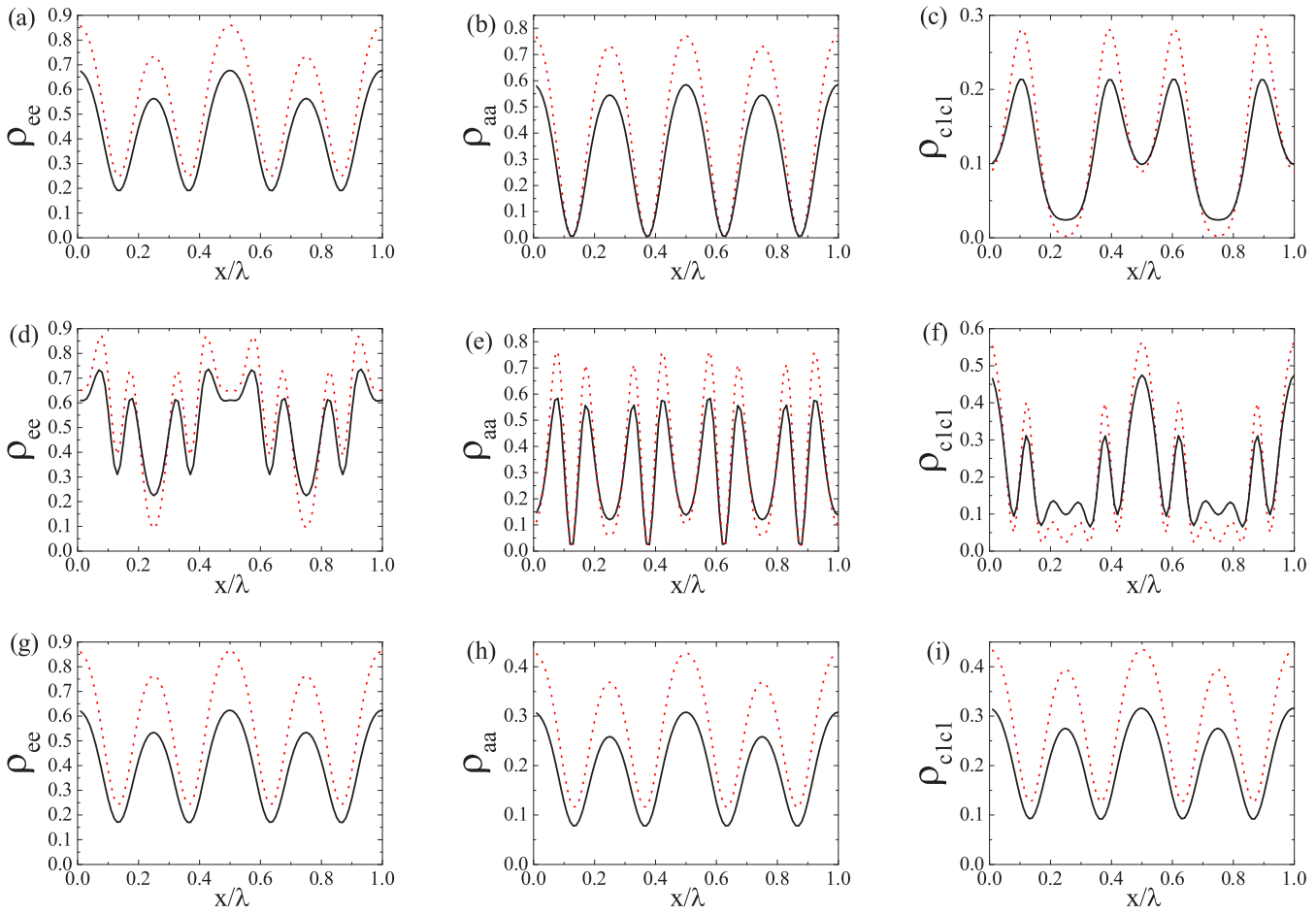

FIG. 2. Probability in the excited states as a function of position x. Decay is excluded in the dashed curve, and included in the solid curve, wavelength $\lambda = 736$ nm. Interaction time $t_0 = 1$ ns, $\Delta_{1+} = -1.1(\omega_a - \omega_{c_2} - \omega_{c_1} + \omega_b) = -691$ GHz, $\Delta_{2+} = 0.9(\omega_a - \omega_{c_2} - \omega_{c_1} + \omega_b) = 565$ GHz, $\Delta_{1-} = -0.9(\omega_a - \omega_{c_2} - \omega_{c_1} + \omega_b) = -565$ GHz, $\Delta_{2-} = 1.1(\omega_a - \omega_{c_2} - \omega_{c_1} + \omega_b) = 691$ GHz, $\rho_{ee} = \rho_{aa} + \rho_{c_1c_1}$. (a)–(c) Temperature $T = 0.1$ K, $\Omega_S = 260$ GHz, $\Omega_D = 40$ GHz. (d)–(f) $T = 0.1$ K, $\Omega_S = 403$ GHz, $\Omega_D = 0.15\Omega_S = 60.5$ GHz. (g)–(i) $T = 300$ K; other parameters are the same as (a).

where H_I is given by Eq. (2) and $\mathscr{L}[\rho]$ is the relaxation of the system which is given by (see details in Appendix)

$$\mathscr{L}[\rho] = -\sum_i \frac{\Gamma_i}{2}[\sigma_+^i\sigma_-^i\rho - \sigma_-^i\rho\sigma_+^i + \text{H.c.}], \qquad (4)$$

where Γ_i is the decay rate of the transition i and $\sigma_\pm^i$ is the raising or lowering operator for the transition i. Due to the orbital relaxation, the electrons on $|a\rangle$ and $|c_2\rangle$ also decay into $|c_1\rangle$ and $|b\rangle$, respectively. The excited state lifetime below 20 K is $\tau = 1.5$ ns so that decay rate $\Gamma_{c_1\to c_2} = \Gamma_{c_1\to b} = \Gamma_{a\to c_2} = \Gamma_{a\to b} = 0.5\tau^{-1}$. The orbital relaxation rate scales linearly with temperature and can be found in Ref. [26].

According to the Boltzmann distribution, nearly all (above 99.99%) electrons are initially in the ground states $|b\rangle$ at low temperature (∼0.1 K) and the orbital relaxation time $T_1 = 40$ ns. The initial condition for Eq. (3) is therefore $\rho_{bb} = 1$ and $\rho_{ij} = 0$ for the other matrix elements. The numerical results for different parameters are shown in Fig. 2. Considering that detection laser may not resolve the upper two energy levels, we also plot the spatial distribution of the total upper-level populations ($\rho_{ee} = \rho_{aa} + \rho_{c_1c_1}$) which are shown in Figs. 2(a), 2(d) and 2(g). In Fig. 2(b), $\frac{\lambda}{4}$ patterns are achieved with a visibility of $V = 1$ and an excitation efficiency of 58%. It is worth noting that, although the perturbation theory is no longer valid ($|\Omega_{\text{eff}}t| = |\frac{\Omega_S^2\Omega_D}{\Delta_{1\pm}\Delta_{2\pm}}t| \approx 5.4 > 1$), the $\frac{\lambda}{4}$ fringes are still nearly perfect sinusoidal without any background noise. This is because $\Omega_D \ll \omega_{ab} - \nu_D$ so that the direct transition $|b\rangle \to |a\rangle$ is almost completely suppressed. We also show the population distribution in state $|c_1\rangle$ which is shown in Figs. 2(c), 2(f) and 2(i). The population in state $|c_1\rangle$ is not completely suppressed because the signal field is not in the perturbation regime. The excitation structure of the state $|c_1\rangle$ is shifted from that of the state $|a\rangle$. Thus, the population on the excited doublets ρ_{ee} has a reduced visibility which is shown in Fig. 2(a). The visibility is reduced from 100% to 57%. Figures 2(e) and 2(f) show the results when we increase the Rabi frequencies. We can see that the $\frac{\lambda}{8}$ pattern is generated. The resolution is doubled because the excited state $|a\rangle$ has undergone a Rabi oscillation.

We also study the temperature's influence on our subwavelength pattern. At room temperature $T = 300$ K, the excited state lifetime is 1.1 ns, and the initial state according to the Boltzmann distribution is $\rho_{bb} = 0.502$ and $\rho_{c_2c_2} = 0.498$. The results are shown in Figs. 2(f)–2(i). The visibility is 0.57, 0.55,

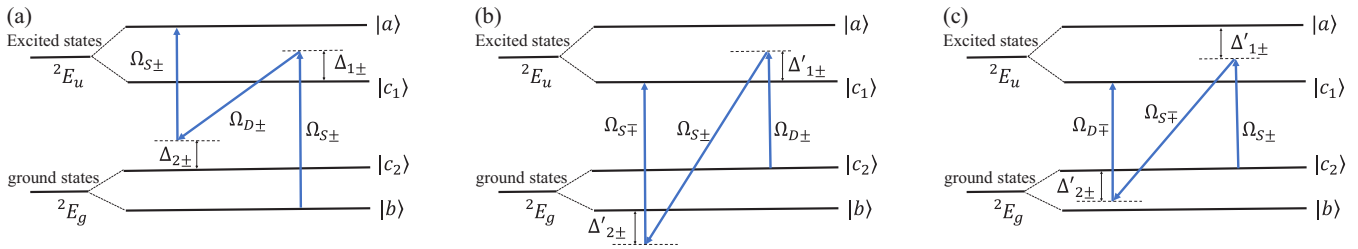

FIG. 3. Three ways of forming $\frac{\lambda}{4}$ fringes. (a) Transition $|b\rangle \to |c_1\rangle \to |c_2\rangle \to |a\rangle$ is achieved by absorbing two photons from the left (right) with frequency ν_+ (ν_-) and one photon from the drive field with frequency ω_+ (ω_-). (b) Transition $|c_2\rangle \to |c_1\rangle \to |b\rangle \to |c_1\rangle$ is achieved by absorbing one photon from the drive field, followed by absorbing one photon from the left (right) and emitting one photon from the right (left). $\Delta'_{1\pm} = \omega_{c_1c_2} - \omega_{D\pm} = \mp 125$ GHz, $\Delta'_{2\pm} = \omega_{c_1b} - \nu_\mp$, $\Delta'_{2+} = -565$ GHz, $\Delta'_{2-} = -691$ GHz. (c) Transition $|c_2\rangle \to |a\rangle \to |c_2\rangle \to |c_1\rangle$ is achieved by first absorbing one photon from the left (right) and emitting one photon from the right (left), then absorbing one photon from the drive field. $\Delta'_{1\pm} = \omega_{ac_2} - \nu_\pm$, $\Delta'_{1+} = 565$ GHz, $\Delta'_{1-} = 691$ GHz, $\Delta'_{2\pm} = \omega_{c_1c_2} - \omega_{D\mp} = \pm 125$ GHz.

0.56 for patterns formed by $|a\rangle$, $|c_1\rangle$, and the excited doublets, respectively, which is higher than the usual method through two-photon absorption in Ref. [22]. $\frac{\lambda}{4}$ fringes on $|a\rangle$ are formed through the $|b\rangle \to |c_1\rangle \to |c_2\rangle \to |a\rangle$ transition pathway with two photons absorbed from $\nu_+(\nu_-)$ and one photon absorbed from $\omega_+(\omega_-)$, as shown in Fig. 3(a). $\frac{\lambda}{4}$ fringes on $|c_1\rangle$ can be formed in two ways, which are shown in Figs. 3(b) and 3(c). Both ways involve the absorption of one photon from the signal beam in one direction and the emission of one photon from the signal beam in the other direction. They are also resonant as long as $\Delta_{1+} + \Delta_{1-} = -(\omega_a - \omega_{c_2} - \omega_{c_1} + \omega_b)$ and $\Delta_{2+} + \Delta_{2-} = \omega_a - \omega_{c_2} - \omega_{c_1} + \omega_b$. Therefore, their patterns are shown to be of the form,

$$|e^{i(k_1+k_2)x} + e^{-i(k_1+k_2)x}| \sim \cos(2(k_1+k_2)x). \tag{5}$$

In Fig. 3(b), the electron is excited from $|c_2\rangle$ to $|c_1\rangle$ by absorbing one photon from the drive field, followed by emitting and absorbing one photon from the signal field to achieve the $|c_1\rangle \to |b\rangle \to |c_1\rangle$ transition. This process is resonant since $\omega_{c_2c_1} = \omega_\pm - \nu_\pm + \nu_\mp$. In Fig. 3(c), the electron undergoes the $|c_2\rangle \to |a\rangle \to |c_2\rangle$ transition by absorbing one photon from one signal beam and emitting one photon from the other signal beam, followed by absorbing one photon from the drive field so it can be pumped to the $|c_1\rangle$ state. This process is also resonant since $\omega_{c_2c_1} = \nu_\pm - \nu_\mp + \omega_\mp$. The noise of Figs. 2(h) and 2(i) is due to the single photon process $|c_2\rangle \to |a\rangle$ and $|b\rangle \to |c_1\rangle$. Therefore, at room temperature, the $\frac{\lambda}{4}$ patterns are formed on $|a\rangle$ and $|c_1\rangle$, and the overall $\frac{\lambda}{4}$ fringes are formed on the excited doublets with a visibility of 0.58 and an efficiency of 0.62.

For lithography, we then need to transfer the internal state population to the photoresist pattern. To achieve this, one may cover the SiV with a thin layer of photoresist. After the above process, the required pattern is mapped to the spatial distribution of the excited state of the SiV system. To transfer this pattern to the resist there are two possible mechanisms: (1) The SiV^- can be ionized by a second laser and the electron would leave the diamond and form a solvated electron on the resist that would drive an electrochemical reaction [33]; (2) a two-color gated photo resist [32] is used to prevent the strong excitation lasers from exposing while allowing the much weaker fluorescence to expose. By the above process, the required pattern can be imprinted to the photoresist.

V. CONCLUSION

We numerically show that the SiV system is a good candidate material for demonstrating the subwavelength optical lithography via classical light. In our numerical calculation, we use the existing material parameters and consider all the allowed transitions. In addition, we also include the decay in our calculation and give a set of parameters to get the $\frac{\lambda}{4}$ pattern with visibility $V = 1$ and efficiency 58% at low temperature. Higher Rabi frequencies and interaction time can compromise the $\frac{\lambda}{8}$ pattern due to higher order effects. Even at room temperature, $\frac{\lambda}{4}$ with a visibility of around 0.57 can be achieved. Due to the similarities in symmetry and electronic structure, this method can be applied to other color centers with suitable parameters.

ACKNOWLEDGMENT

This work is supported by a grant from the Qatar National Research Fund (QNRF) under NPRP Project No. 8-352-1-074.

APPENDIX: DERIVATION OF EQ. (3)

We now generalize the decay between the two-level system to the multilevel system. The interaction Hamiltonian for the multilevel system is

$$V(t) = \hbar \sum_{i,\boldsymbol{k}} g_{\boldsymbol{k},i}(a^\dagger_{\boldsymbol{k}} \sigma^i_- e^{-i(\omega_i - \nu_{\boldsymbol{k}})t} + \sigma^i_+ a_{\boldsymbol{k}} e^{i(\omega_i - \nu_{\boldsymbol{k}})t}), \tag{A1}$$

where $g_{\boldsymbol{k},i} = \sqrt{\frac{\nu_{\boldsymbol{k}}}{2\hbar\epsilon_0 V}}\mu_i \cos\theta$, μ_i is the dipole magnitude for transition i, and θ is the angle between the atomic dipole direction and electric field polarization vector. Since the lifetime in the excited states is around 1 ns, we can approximate the linewidth as 1 GHz, which is much smaller than the splitting between the ground doublets ~50 GHz. Therefore, we can rewrite Eq. (B1) as

$$V(t) = \hbar \sum_{i,\boldsymbol{k}} g_{\boldsymbol{k},i}(a^\dagger_{\boldsymbol{k},i} \sigma^i_- e^{-i(\omega_i - \nu_{\boldsymbol{k},i})t} + \sigma^i_+ a_{\boldsymbol{k},i} e^{i(\omega_i - \nu_{\boldsymbol{k},i})t}), \tag{A2}$$

where the subscript i means the photon is from transition i, so we have $[a_{\boldsymbol{k},i}, a^\dagger_{\boldsymbol{k},j}] = \delta_{i,j}$. The physical meaning is easy to understand: The Lorentzians of each decay have no overlap, so that the photon from transition i cannot be the photon from transition j. Then we insert Eq. (B2) into the equation of

motion for the reduced density matrix of the system ρ_S [34],

$$\dot{\rho_S} = -\frac{i}{\hbar}\mathrm{Tr}_R[V(t),\rho_S(0)\otimes\rho_R(0)] - \frac{1}{\hbar^2}\mathrm{Tr}_R\int_0^t [V(t),[V(t'),\rho_S(t')\otimes\rho_R(0)]]dt', \quad \text{(A3)}$$

where ρ_R is the density matrix for the vacuum reservoir. For the vacuum reservoir we have $\langle a_{\boldsymbol{k},i}\rangle = \langle a^\dagger_{\boldsymbol{k},i}\rangle = 0, \langle a_{\boldsymbol{k},i}a^\dagger_{\boldsymbol{k}',j}\rangle = \delta_{\boldsymbol{k}\boldsymbol{k}'}\delta_{ij}, \langle a^\dagger_{\boldsymbol{k},i}a_{\boldsymbol{k}',j}\rangle = 0, \langle a_{\boldsymbol{k},i}a_{\boldsymbol{k}',j}\rangle = \langle a^\dagger_{\boldsymbol{k},i}a^\dagger_{\boldsymbol{k}',j}\rangle = 0$. Then trivial calculation leads to

$$\begin{aligned}\dot{\rho_S} &= -i\sum_{i,\boldsymbol{k}} g_{\boldsymbol{k},i}\mathrm{Tr}_R(a^\dagger_{\boldsymbol{k},i}\rho_R)[\sigma^i_-,\rho_S(0)]e^{-i(\omega_i-\nu_{\boldsymbol{k},i})t} - \int_0^t dt'\sum_{i',\boldsymbol{k}',i,\boldsymbol{k}} g_{\boldsymbol{k},i}g_{\boldsymbol{k}',i'}\{[\sigma^i_-\sigma^{i'}_-\rho_S(t') - 2\sigma^{i'}_-\rho_S(t')\sigma^i_- + \rho_S(t')\sigma^i_-\sigma^{i'}_-] \\ &\times e^{-i(\omega_i-\nu_{\boldsymbol{k},i})t-i(\omega_{i'}-\nu_{\boldsymbol{k}',i'})t'}\mathrm{Tr}_R(a^\dagger_{\boldsymbol{k},i}a^\dagger_{\boldsymbol{k}',i'}\rho_R) + [\sigma^i_-\sigma^{i'}_+\rho_S(t') - \sigma^{i'}_+\rho_S(t')\sigma^i_-]e^{-i(\omega_i-\nu_{\boldsymbol{k},i})t+i(\omega_{i'}-\nu_{\boldsymbol{k}',i'})t'}\mathrm{Tr}_R(a^\dagger_{\boldsymbol{k},i}a_{\boldsymbol{k}',i'}\rho_R) \\ &+ [\sigma^i_+\sigma^{i'}_- - \sigma^{i'}_-\sigma^i_+]e^{i(\omega_i-\nu_{\boldsymbol{k},i})t-i(\omega_{i'}-\nu_{\boldsymbol{k}',i'})t'}\mathrm{Tr}_R(a_{\boldsymbol{k},i}a^\dagger_{\boldsymbol{k}',i'}\rho_R)\} + \mathrm{H.c.} \\ &= -\sum_{i,\boldsymbol{k}}\int_0^t dt' g^2_{\boldsymbol{k},i}[\sigma^i_+\sigma^i_-\rho_S(t') - \sigma^i_-\rho_S(t')\sigma^i_+]e^{i(\omega-\nu_{\boldsymbol{k},i})(t-t')} + \mathrm{H.c.} \end{aligned} \quad \text{(A4)}$$

We replace $\sum_{i,\boldsymbol{k}}$ by $2\frac{V}{(2\pi)^3}\int_0^{2\pi}d\phi\int_0^{\pi}d\theta\sin\theta\int_0^{\infty}dkk^2$ where factor 2 is for two polarizations, V is the quantization volume, and $k = \frac{\omega}{c}\sqrt{\epsilon_r\mu_r}$. Then we use the Weisskopf-Wigner approximation, and we can get

$$\dot{\rho} = -\sum_i\frac{\Gamma_i}{2}[\sigma^i_+\sigma^i_-\rho - \sigma^i_-\rho\sigma^i_+ + \mathrm{H.c.}], \quad \text{(A5)}$$

where $\Gamma_i = \frac{1}{4\pi\epsilon_o}\frac{4\omega^3\mu_i^2}{3\hbar c^3}$. Considering this process occurs in diamond, we need to replace Γ_i by the decay rate in the medium: $\Gamma'_i = \frac{(n(\omega))^3}{\epsilon_r(\omega)}\Gamma_i$ [35]. Then we get Eq. (4).

[1] S. R. J. Brueck, S. H. Zaidi, X. Chen, and Z. Zhang, Microelectron. Eng. **41–42**, 145 (1998).
[2] M. Madou, *Fundamentals of Microfabrication* (CRC Press, Boca Raton, 2002).
[3] C. Mack, *Fundamental Optical Principles of Lithography: The Science of Microfabrication* (John Wiley & Sons, West Sussex, 2007).
[4] C. Williams *et al.*, Inf. Forsch. Ent. **21**, 73 (2006).
[5] M. Al-Amri, Z. Liao, and M. S. Zubairy, in *Advances in Atomic, Molecular, and Optical Physics*, Vol. 61, edited by E. Arimondo, P. R. Berman, and C. C. Lin (Academic Press, Cambridge, 2012), pp. 409–466.
[6] P. R. Hemmer and T. Zapata, J. Opt. **14**, 083002 (2012).
[7] M. D'Angelo, M. V. Chekhova, and Y. Shih, Phys. Rev. Lett. **87**, 013602 (2001).
[8] I. Afek, O. Ambar, and Y. Silberberg, Science **328**, 879 (2010).
[9] O. Steuernagel, J. Opt. B: Quantum Semiclass. Opt. **6**, S606 (2004).
[10] G. S. Agarwal and K. T. Kapale, J. Phys. B **39**, 3437 (2006).
[11] M. Kiffner, J. Evers, and M. S. Zubairy, Phys. Rev. Lett. **100**, 073602 (2008).
[12] H. Li, V. A. Sautenkov, M. M. Kash, A. V. Sokolov, G. R. Welch, Y. V. Rostovtsev, M. S. Zubairy, and M. O. Scully, Phys. Rev. A **78**, 013803 (2008).
[13] Z. Liao, M. Al-Amri, and M. S. Zubairy, Phys. Rev. Lett. **105**, 183601 (2010).
[14] Z. Liao, M. Al-Amri, and M. S. Zubairy, J. Phys. B: At. Mol. Opt. Phys. **48**, 105101 (2015).
[15] J. Rui, Y. Jiang, G.-P. Lu, M.-J. Zhu, B. Zhao, X.-H. Bao, and J.-W. Pan, Phys. Rev. A **93**, 033837 (2016).
[16] Z. Liao, M. Al-Amri, T. Becker, W. P. Schleich, M. O. Scully, and M. S. Zubairy, Phys. Rev. A **87**, 023405 (2013).
[17] Z. Liao, M. Al-Amri, and M. S. Zubairy, Phys. Rev. A **88**, 053809 (2013).
[18] M. F. Fouda, R. Fang, J. B. Ketterson, and M. S. Shahriar, Phys. Rev. A **94**, 063644 (2016).
[19] F. AlGhannam, P. Hemmer, Z. Liao, and M. S. Zubairy, Technologies **4**, 12 (2016).
[20] G. S. Agarwal, R. W. Boyd, E. M. Nagasako, and S. J. Bentley, Phys. Rev. Lett. **86**, 1389 (2001).
[21] P. R. Hemmer, A. Muthukrishnan, M. O. Scully, and M. S. Zubairy, Phys. Rev. Lett. **96**, 163603 (2006).
[22] S. J. Bentley and Robert W. Boyd, Opt. Express **12**, 5735 (2004).
[23] Q. Sun, P. R. Hemmer, and M. S. Zubairy, Phys. Rev. A **75**, 065803 (2007).
[24] W. Ge, P. R. Hemmer, and M. S. Zubairy, Phys. Rev. A **87**, 023818 (2013).
[25] A. T. Collins, L. Allers, C. J. Wort, and G. A. Scarsbrook, Diamond Relat. Mater. **3**, 932 (1994).
[26] K. D. Jahnke, A. Sipahigil, J. M Binder, M. W. Doherty, M. Metsch, L. J. Rogers, N. B. Manson, M. D. Lukin, and F. Jelezko, New J. Phys. **17**, 043011 (2015).
[27] T. Iwasaki, F. Ishibashi, Y. Miyamoto, Y. Doi, S. Kobayashi, T. Miyazaki, K. Tahara, K. D. Jahnke, L. J. Rogers, B. Naydenov, F. Jelezko, S. Yamasaki, S. Nagamachi, T. Inubushi, N. Mizuochi, and M. Hatano, Sci. Rep. **5**, 12882 (2015).
[28] M. W. Doherty, N. B. Manson, P. Delaney, F. Jelezko, J. Wrachtrup, and L. C. L. Hollenberg, Phys. Rep. **528**, 1 (2013).

[29] J. Michl, T. Teraji, S. Zaiser, I. Jakobi, G. Waldherr, F. Dolde, P. Neumann, M. W. Doherty, N. B. Manson, J. Isoya, and J. Wrachtrup, Appl. Phys. Lett. **104**, 102407 (2014).

[30] C. D. Clark, H. Kanda, I. Kiflawi, and G. Sittas, Phys. Rev. B **51**, 16681 (1995).

[31] L. J. Rogers, K. D. Jahnke, M. W. Doherty, A. Dietrich, L. P. McGuinness, C. Müller, T. Teraji, H. Sumiya, J. Isoya, N. B. Manson, and F. Jelezko, Phys. Rev. B **89**, 235101 (2014).

[32] R. R. McLeod, B. A. Kowalski, and M. C. Cole, Proc. SPIE **7591**, 759102 (2010).

[33] D. Zhu, L. Zhang, R. E. Ruther, and R. J. Hamers, Nat. Mater. **12**, 836 (2013).

[34] M. O. Scully and M. S. Zubairy, *Quantum Optics* (Cambridge University Press, Cambridge, 1997).

[35] G. Nienhuis and C. Th. J. Alkemade, Physica C **81**, 181 (1976).